Heliyon 10 (2024) e27630

Contents lists available at ScienceDirect

Heliyon

journal homepage: www.cell.com/heliyon

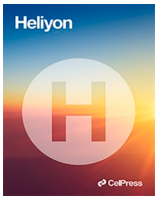

Research article

Immunogenic cell death related mRNAs associated signature to predict immunotherapeutic response in osteosarcoma

Shuai Han [1], Qinghe Wang [1], Mingquan Shen [1], Xingpeng Zhang, Jian Wang [*]

Department of Orthopedics, Shanghai Pudong New Area People's Hospital, Shanghai, 201299, China

A R T I C L E I N F O

Keywords:
Osteosarcoma
Oxidative stress
Immunogenic cell death
Tumor microenvironment
Risk signature

A B S T R A C T

Background: Immunogenic cell death (ICD) is related to cancer prognosis, which has a synergic effect in combination with chemotherapy or immunotherapy. Yet, the relationship between ICD and osteosarcoma remained unclear.

Materials and methods: Three osteosarcoma datasets including therapeutically applicable research to generate effective treatments (TARGET), GSE126209 and GSE21257 datasets were included. A protein-protein interaction network was constructed based on ICD-related genes. We performed unsupervised consensus clustering to classify molecular subtypes (clusters). Survival analysis, Estimation of stromal and immune cells in malignant tumour tissues using expression data (ESTIMATE), Cell-type identification by estimating relative subsets of RNA transcripts (CIBERSORT), and differential analysis were employed to characterize the molecular differences between different clusters. Univariate Cox regression analysis was conducted to confirm prognostic genes. Quantitative reverse transcription polymerase chain reaction (qRT-PCR) was used to demonstrate the aberrant expression of ICD-correlated signature genes in osteosarcoma. A series of cellular experiments, including cell counting kit-8 (CCK-8), transwell, and flow cytometry, were used to demonstrate the regulatory role of key genes in the ICD model on the malignant phenotype of osteosarcoma.

Results: Three clusters (cluster1, 2, 3) were constructed and they showed distinct overall survival and immune infiltration. ICD-related genes were highly expressed in cluster1. Moreover, Cluster1 had the best prognosis, high immune score and high expression of human leukocyte antigen (HLA)-related genes. *TLR4*, *LY96*, *IFNGR1*, *CD4*, and *CASP1* were identified as prognostic genes for establishing an ICD-related risk signature. According to the risk signature, two risk groups (high and low risks) showing differential prognosis and response to immunotherapy. The low risks group had a better prognosis but was not sensitive to immunotherapy. Molecular assays verified that prognostic genes were abnormally under-expressed in osteosarcoma. Cellular assays demonstrated that LY96, the most significantly down-regulated gene in osteosarcoma, inhibited the migration, invasion, and proliferation phenotypes of osteosarcoma cells and prolonged the cell cycle. Analysis of oxidative stress related pathway enrichment in tumor microenvironment was conducted by single-sample gene set enrichment analysis (ssGSEA).

Conclusions: This study demonstrated the prognostic significance of ICD-correlated genes in osteosarcoma patients. The five-gene risk signature facilitate prognostic evaluation and prediction

* Corresponding author. Department of Orthopedics, Shanghai Pudong New Area People's Hospital, China.
E-mail address: wjwj0328@163.com (J. Wang).
[1] Equal Contribution.

https://doi.org/10.1016/j.heliyon.2024.e27630
Received 4 December 2023; Received in revised form 3 March 2024; Accepted 4 March 2024
Available online 9 March 2024

of osteosarcoma patients' response to immunotherapy. The risk signature also offered a possibility for the exploit of novel ICD-related treatment.

1. Introduction

Osteosarcoma is a rare bone tumor derived from malignant mesenchymal cells, which occurs mostly in adolescent patients between 5 and 15 years old [1,2]. Another incidence peak is in the older patients aging more than 65 [3]. Paget disease and radiation are two major causes of osteosarcoma [4,5]. Osteosarcoma as the most frequent primary tumor type in bone tumor, which largely affects in the sites of distal femur and proximal tibia [6,7]. In the twentieth century, the five-year overall survival of osteosarcoma was about 20% [8]. While in the late 20th century, the overall survival rate reached 50% under the adjuvant chemotherapy [9–11]. At the same time, the treatment of osteosarcoma changed to chemotherapy and limb salvage. The current therapy of osteosarcoma involves neoadjuvant or adjuvant chemotherapy, surgical resection, and the emphasis on continuous treatment after resection [12]. However, metastatic patients contribute to the most of death and have a dramatically lower survival rate (less than 20%) compared to non-metastatic patients [13]. Although chemotherapy increases the survival rate of osteosarcoma patients, the efficiency is extremely low and it is destructive to the whole body with a series of side effects, Semiconductor polymer nanoparticles derived from emerging photothermal therapy and photodynamic therapy exhibited significant anti-tumor activity and low toxicity [14]. In particular, immunotherapies including immunomodulators represented by interleukin-2 and cytidylic tripeptides, dendritic cells, immune checkpoint inhibitors, and engineered T cells show promising prospects in antitumor therapy [15]. Despite the current lack of some reliable immunotherapeutic markers, Zhang et al. identified a subpopulation of cells that can that enhance T-cell toxicity in *anti*-PD-L1 therapy in osteosarcoma patients by single-cell technology, offering hope for improved patient prognosis [16]. Usually, the innate and adaptive immune system response to tumor cells through the signals such as cytokines and tumor-specific antigens, and then kill tumor cells. However, the immune surveillance not always works due to some tumor cells escaping from immune system [15]. For example, myeloid-derived suppressor cells (MDSC) are present in the immunosuppressive tumor microenvironment, and therapies targeting MDSC have shown positive results [17]. Novel nanomaterial-based antitumor drugs have shown extremely high targeting properties unlike highly toxic chemotherapeutic drugs [18]. Immunotherapies based on neoantigen-reactive T-cell function also show promising prospects in solid tumors [19]. To rescuing the immune response to tumor cells, various strategies including dendritic cell vaccine [20], chimeric antigen receptor (CAR)-T cell therapy [21], and immune checkpoint inhibitors [22,23] have been developed and some have been under clinical trials in osteosarcoma patients [24]. Among these immunotherapies, immune checkpoint blockade reaches a breakthrough in treating various cancer types, which is promising to treat metastatic cancer. Nevertheless, the positive responsive rate of immune checkpoint inhibitors remains an obstacle and thus effective indicators should be developed for guiding personalized immunotherapy.

The role of immunogenic cell death (ICD) in cancer involves a process in which dead tumor cells release or are exposed to damage-associated molecular patterns (DAMPs) [25]. During ICD, tumor cells released or express a series of molecules DAMPs, such as calreticulin, heat shock proteins, ATP, and HMGB1, upon death. These molecules attract and activate immune cells, such as dendritic cells, which in turn activate T cells that trigger a specific immune response against the tumor. Activation of the cGAS-STING signaling pathway also plays a key role in this process, further promoting an immune response against the tumor. This mechanism is important in tumor therapy, especially in the application of radiotherapy and certain chemotherapeutic agents [26,27]. Excitingly, the nanomaterials address the difficulty of phototherapy-triggered ICDs in eliciting a robust anti-tumor immune response, killing tumor cells by generating large amounts of reactive oxygen species (ROS) [28]. The effects of cancer therapy have been discovered to be associated with the induction of ICD. ICD offers a hope of improving the efficiency of cancer therapy implemented together with immune checkpoint inhibitors [29–31].

With a focus on ICD-related genes (also called DAMP-related genes), this study aimed to reveal the relationship of ICD and immune microenvironment in osteosarcoma. ICD-associated risk profiles predictive of overall survival in osteosarcoma were developed, and the regulatory role of the characteristic genes in osteosarcoma progression was validated by cellular experiments.

2. Materials and Methods

2.1. Acquisition and preprocessing of data

We accessed the expression profiles and clinical data of osteosarcoma samples from UCSC Xena (https://xenabrowser.net/) and Gene Expression Omnibus (GEO, https://www.ncbi.nlm.nih.gov/geo/). TARGET dataset was downloaded from UCSC Xena in June 27, 2022. GSE126209 and GSE21257 datasets were obtained from GEO database in June 27, 2022. For TARGET dataset, we transferred Ensembl ID to gene symbol through "gencode.v22.annotation.gene.probeMap". Fragments per kilobase million (FPKM) was transferred to transcripts per million (TPM), and log2(TPM) expression was used for the analysis. For GSE126209 and GSE21257 datasets, we converted the probes to gene symbols and selected the averaged value of expression of a gene with multiple probes.

2.2. Protein-protein interaction (PPI) analysis

The evaluation of the gene-gene interaction often applies the methodology of PPI analysis based on the gene interaction data stored

in the public database. We used STRING tool (https://cn.string-db.org/) to conduct PPI analysis of 34 ICD-correlated genes obtained from a previous research [32].

2.3. Molecular subtyping using ICD-correlated genes

We applied unsupervised consensus clustering [33] using expression profiles of ICD-correlated genes for molecular subtyping of osteosarcoma. Distance = "euclidean" and clusterAlg = "pam" parameters were determined to conduct 1000 repeats. The optimal cluster number k was determined from the range of 2–6 on the basis of cumulative distribution function (CDF) and consensus matrix.

2.4. Characterization of immune microenvironment

We used two methodologies (ESTIMATE and CIBERSORT) to estimate the immune infiltration. ESTIMATE [34] was utilized to evaluate the total immune infiltration, stromal infiltration and tumor purity of three clusters by using ESTIMATE R package. CIBERSORT [35] (http://cibersort.stanford.edu/) was applied to quantifying 22 types of immune cells.

2.5. Tumor immune dysfunction and exclusion (TIDE)

TIDE tool [36] (http://tide.dfci.harvard.edu/) was used to predict the clinical responsiveness to immune checkpoint blockade based on the gene expression profiles. TIDE score was calculated based on the T cell exclusion and T cell dysfunction score. TIDE score is positively related to a greater chance of immune escape from immunotherapy. The Tumor Immune Insufficiency and Exclusion (TIDE) score is a computational method designed to predict response to immunotherapy in cancer patients by modeling two major mechanisms of tumor immune evasion: T cell dysfunction and T cell exclusion. Studies have shown that higher TIDE scores are associated with higher immune escape potential and lower immunotherapy response rates, making TIDE scores an important indicator for predicting immunotherapy outcomes. The TIDE score is closely associated with immune evasion and resistance to immunotherapy in the tumor microenvironment, suggesting that it can serve as a surrogate biomarker for assessing response to immunotherapy, including treatments such as *anti*-PD1 and *anti*-CTLA4. Indeed, lower TIDE scores were associated with higher immunotherapy response rates in the patient population, suggesting that patients with lower TIDE scores may benefit more from this type of treatment.

2.6. Differential expression analysis and functional analysis

Limma in the R was here to perform differential expression analysis [37]. Differentially expressed genes (DEGs) were identified between different clusters. ClusterProfiler R package [38] was adopted to conduct functional analysis for identifying significantly enriched GO terms and KEGG pathways. $P < 0.05$ was determined to screen enriched pathways, followed by visualizing the top 10 enriched pathways.

2.7. Establishing and validating an ICD risk signature

Firstly, on the basis of the ICD-correlated genes showing prognosis significance screened by univariate Cox regression analysis, LASSO was performed using glmnet R package [39] to calculate the coefficients of the prognostic genes and establish a risk signature defined as: risk score $= \Sigma \beta i * \text{Expi}$. β indicates the LASSO coefficients and Exp indicates the expressions of the prognostic genes. High-risk and low-risk groups of osteosarcoma samples were stratified by the cut-off of median value of risk score. The performance of the risk signature was evaluated by plotting Kaplan-Meier (KM) curves and performing univariate Cox regression.

2.8. Cell culture and transient transfection

DEME F-12 medium was used to culture MG-63 (BNCC338584), Saos-2 (BNCC338485) and hFOB1.19 (BNCC255176) cells (purchased from Beijing Bena Biotechnology Co. Beijing, China). Cells were transfected with negative control (NC) and Plasmids overexpressing LY96 (Sagon, China) utilizing Lipofectamine 2000 (Invitrogen, Thermo Fisher, USA).

Table 1
The sequences of primers for target genes.

Gene	Forward primer sequence (5′-3′)	Reverse primer sequence (5′-3′)
TLR4	CCCTGAGGCATTTAGGCAGCTA	AGGTAGAGAGGTGGCTTAGGCT
LY96	CCCTGTATAGAATTGAAAGGATCC	TGCGCTTTGGAAGATTCATGGTG
IFNGR1	AGTGCTTAGCCTGGTATTCATCTG	GGCTGGTATGACGTGATGAGTG
CD4	CCTCCTGCTTTTCATTGGGCTAG	TGAGGACACTGGCAGGTCTTCT
CASP1	GCTGAGGTTGACATCACAGGCA	TGCTGTCAGAGGTCTTGTGCTC
GAPDH	AATGGGCAGCCGTTAGGAAA	GCCCAATACGACCAAATCAGAG

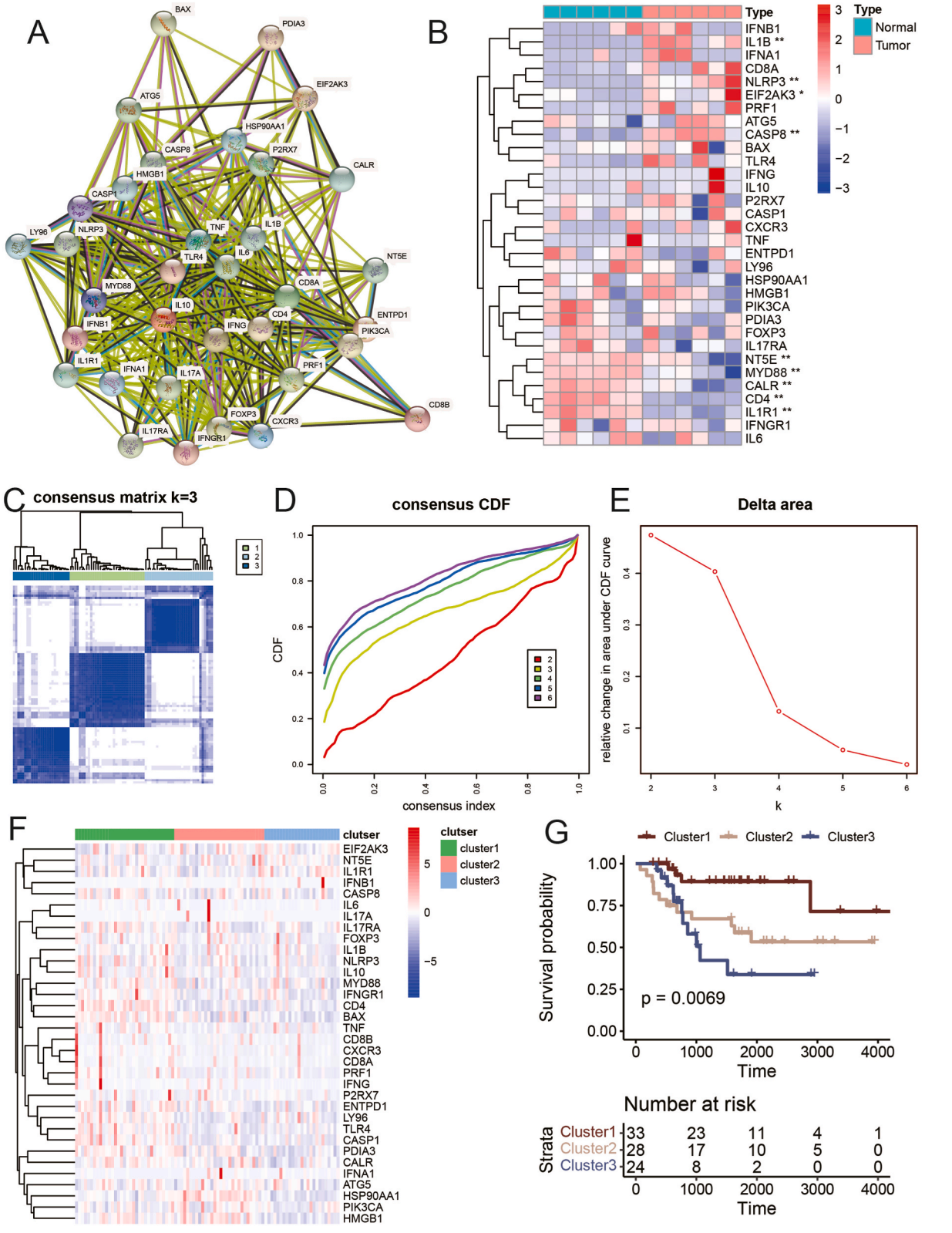

(caption on next page)

Fig. 1. Molecular subtyping based on ICD-correlated genes. (A) A PPI network of 34 ICD-correlated genes in GSE126209 dataset. (B) A heatmap of expression of ICD-correlated genes in osteosarcoma and normal samples in GSE126209 dataset. Student *t*-test was conducted. (C) Consensus clustering when cluster number k = 3 in TARGET dataset. (D–E) Consensus CDF curve when k = 2–6. (F) The expression heamap of 34 ICD-related genes in three clusters in TARGET dataset. (G) Kaplan-Meier survival curve of three clusters in TARGET dataset. Log-rank test was conducted. *P < 0.05, **P < 0.01.

2.9. qRT-PCR

Extraction of total RNA from hFOB1.19, MG-63 and Saos-2 cell lines (Thermo Fisher, USA) was conducted using TRIzol reagent. HiScript II SuperMix (Vazyme, China) was employed to separate cDNA from 500 ng of RNA. QRT-PCR was carried out in ABI 7500 System (Thermo Fisher, USA) with the use of SYBR Green Master Mix and PCR was amplified for 45 cycles at 94 °C for 10 min (min), at 94 °C for 10 s (s), and at 60 °C for 45 s. GAPDH was an internal reference. Primer sequneces for the genes were listed as Table 1.

2.10. Transwell assay

Migration and invasion of MG-63 and Saos-2 cells were detected by carrying out Transwell assay. Chambers coated (for invasion) or uncoated with Matrigel (BD Biosciences, USA) (for migration) were inoculated with cells (5×10^4). Serum-free medium and complete DMEM medium was respectively added to the upper and lower layer. Following 24-h incubation, 4% paraformaldehyde and stained with 0.1% crystalline violet were applied to fix and dye the cells, respectively.

2.11. Cell viability

Cell Counting Kit-8 assay (Beyotime, China) was conducted for assessing cell viability. All the cells (1×10^3 cells/well) were cultured in 96-well plates and added with CCK-8 solution at specific time points. After 2-h incubation at 37 °C, we used a microplate reader (BioTeK, USA) to measure the O.D 450 value of each well.

2.12. Cell cycle

Pre-cooled ethanol (75%) was gently added to MG-63 and Saos-2 cell lines contained in the centrifuge tube overnight at 4 °C. After washing the fixed cells, PI (2 mg/mL) in PBS with RNase A (0.1 mg/mL) was used for cell staining in the dark for 30 min at room temperature. Cell distribution with different DNA content was analyzed applying FACSCalibur flow cytometry (BD Biosciences) and Flowjo software at the excitation wavelength of 530 nm.

2.13. Statistical analysis

Current data analysis was conducted with the help of Sangerbox platform (http://vip.sangerbox.com/) [40]. Difference among three cluster was exmained using Kruskal-Wallis test or ANOVA. KM survival analysis and Cox regression analysis were conducted with log-rank test. Wilcoxon test was performed between two groups. We considered P < 0.05 as significant. The statistical methods were also indicated in the figure legends.

3. Results

3.1. Molecular subtyping for osteosarcoma using ICD-related genes

A total of 34 ICD-related genes were collected from a past research [32], and the PPI analysis showed that these ICD-related genes had tight interactions with each other (Fig. 1A). In GSE126209 dataset, we evaluated the expressions of 34 ICD-correlated genes in six osteosarcoma samples and six normal samples. A heatmap presented the expression patterns of the total 34 in all samples. Among 34 genes, nine of them had a significant difference of expression between osteosarcoma and normal samples, including *IL1B*, *NLRP3*, *EIF2AK3*, *CASP8*, *NT5E*, *MYD88*, *CALR*, *CD4* and *IL1R1* (P < 0.05, Fig. 1B). Next, a consensus matrix was developed on the basis of the expression of these genes by consensus clustering in TARGET dataset. According to the consensus CDF, cluster number k = 3 was determined to divide samples into three clusters (Fig. 1C–E). Three clusters (cluster1, 2, and 3) showed different expression patterns of 34 genes (Fig. 1F). In addition to the expression pattern, three clusters also exhibited differential overall survival, where cluster1 had the longest overall survival and cluster3 had the shortest (P = 0.0069, Fig. 1G).

3.2. Differential immune infiltration and responses to immunotherapy of three clusters

ICD induces immune-mediated elimination in the tumor microenvironment (TME) and reshape the TME [41]. Therefore, we assessed whether a difference of immune infiltration was shown among three clusters. We compared the immune infiltration, stromal infiltration, and tumor purity in three clusters, and we found that cluster1 had the highest score of immune infiltration, but the lowest purity of tumor (Fig. 2A–C). Moreover, CIBERSORT analysis revealed that M0 macrophages, activated memory CD4 T cells, naïve CD4

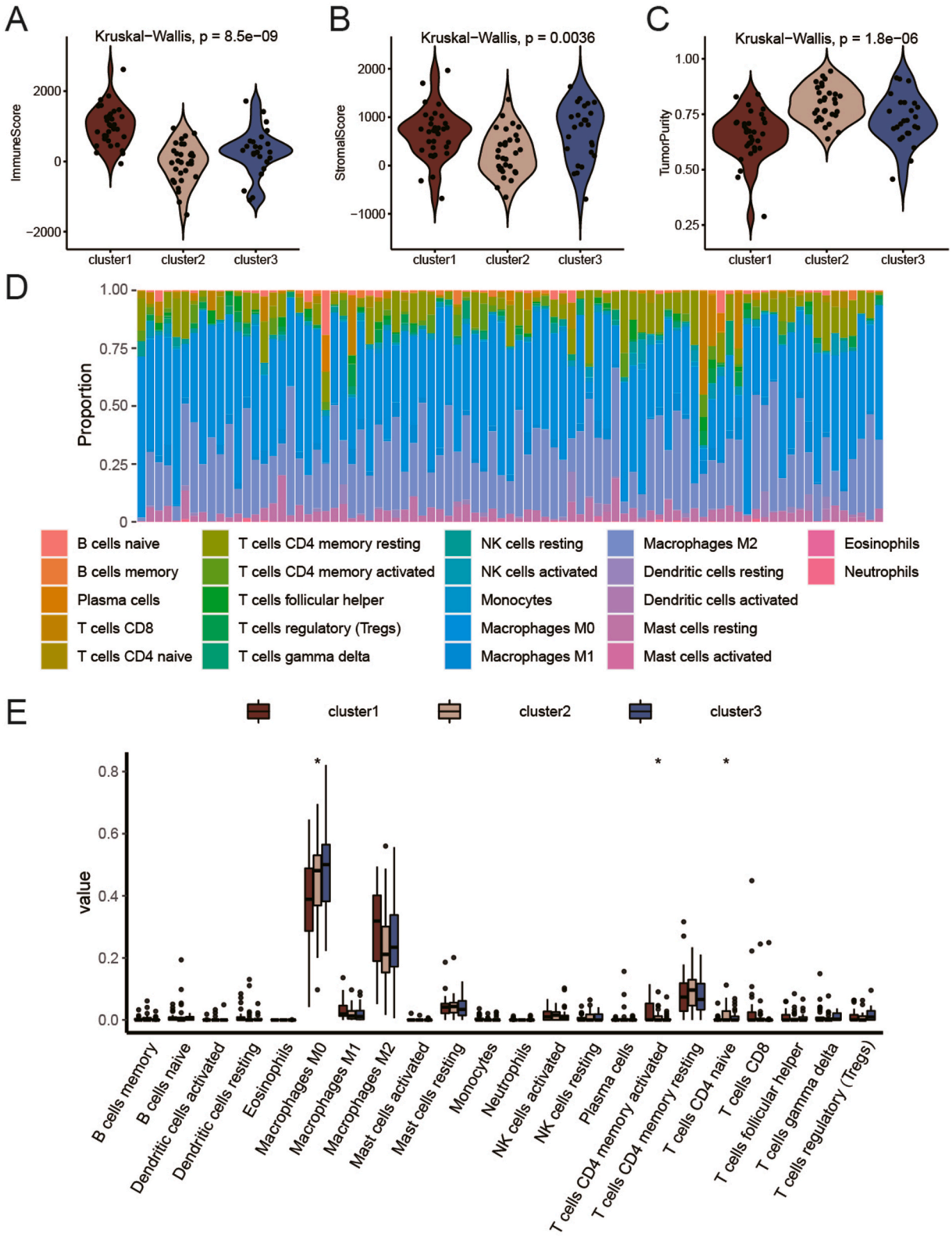

Fig. 2. The immune analysis of three clusters in TARGET dataset. (A–C) The tumor purity, immune score, stromal score of three clusters. (D) The distribution of 22 immune cells. (E) Comparison of the enrichment score of 22 immune cells in three clusters. Kruskal-Wallis test was conducted. *P $<$ 0.05.

T cells were differentially enriched in three clusters, where cluster1 had the lowest proportion of M0 macrophages and the highest proportion of activated memory CD4 T cells (Figs. 2D and 1E). Additionally, the expression of human leukocyte antigen (HLA)-associated genes and immune checkpoint genes were evaluated. Two immune checkpoints (HAVCR2 and LAG3) had significantly higher expression levels in cluster1 with P = 1.9e-06 and P = 0.0099 respectively (Fig. 3A and B). Notably, HLA-associated genes differentially expressed in three clusters (Fig. 3C), indicating that three clusters may have different immune response to immune checkpoint blockade therapy.

3.3. Functional analysis of DEGs among three clusters

In the previous sections, we illustrated that three clusters had different expression patterns of ICD-correlated genes, different overall survival, and different TME. Furthermore, we identified DEGs between clusters by using differential analysis. We plotted Venn plot using the ggvenn package. Venn plot demonstrated a total of 68 DEGs and a heatmap presented the expression patterns of the 68 DEGs in three clusters (Fig. 4A and B). Specially, most of DEGs were relatively upregulated in cluster1. Functional analysis on the 68 DEGs revealed that antigen processing and presentation, extracellular exosome, and MHC class II protein complex were mostly enriched (Fig. 4C and D). In combination with the above findings, we suspected that ICD-related genes were involved in the regulation of immune microenvironment and thus affected the progression of osteosarcoma.

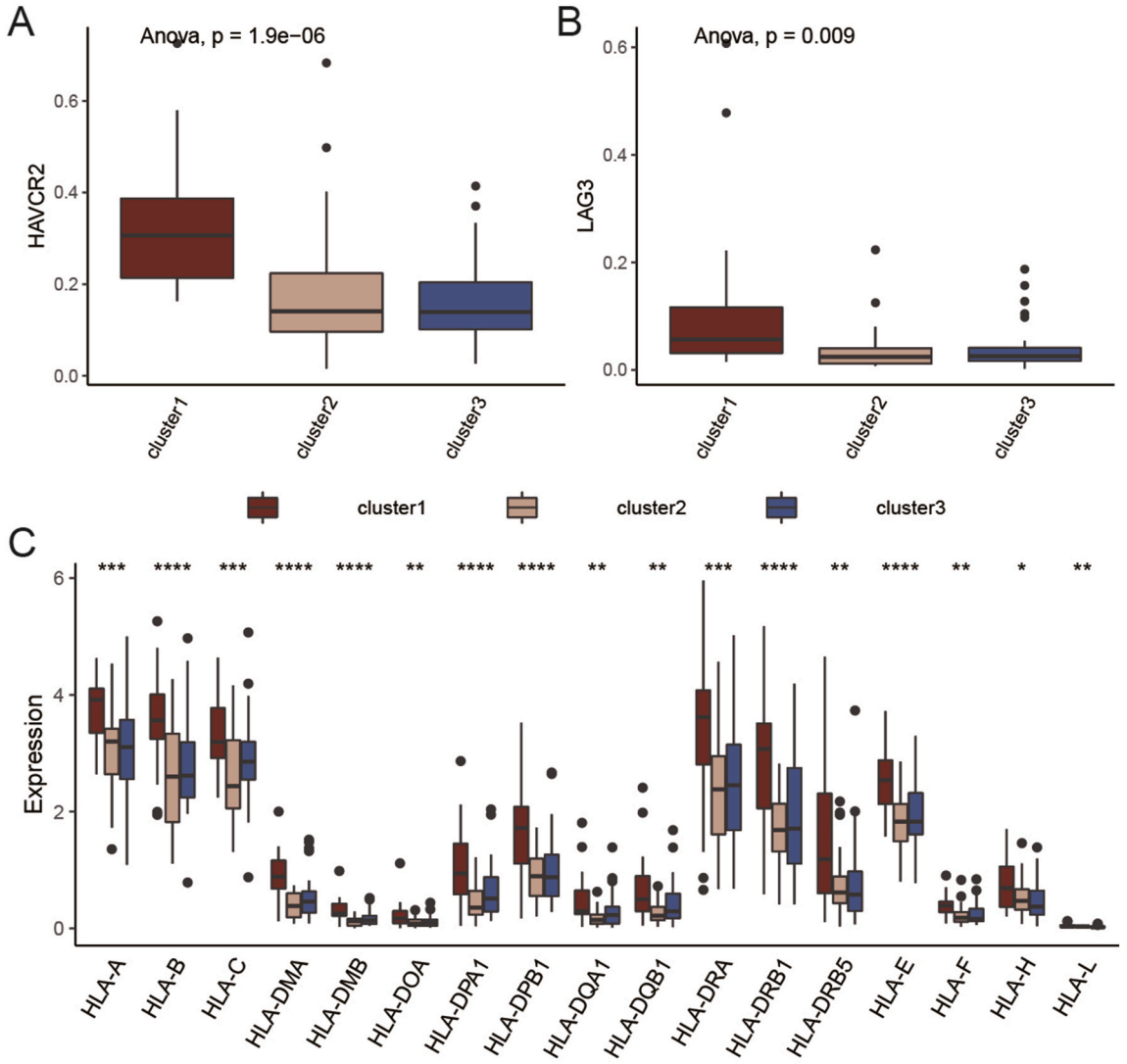

Fig. 3. The immune response of three clusters in TARGET dataset. (A–B) The expression of two immune checkpoints, HAVCR2 and LAG3 in three clusters. (C) The expression of HLA-related genes in three clusters. ANOVA test was conducted. *P < 0.05, **P < 0.01, ***P < 0.001, ****P < 0.0001.

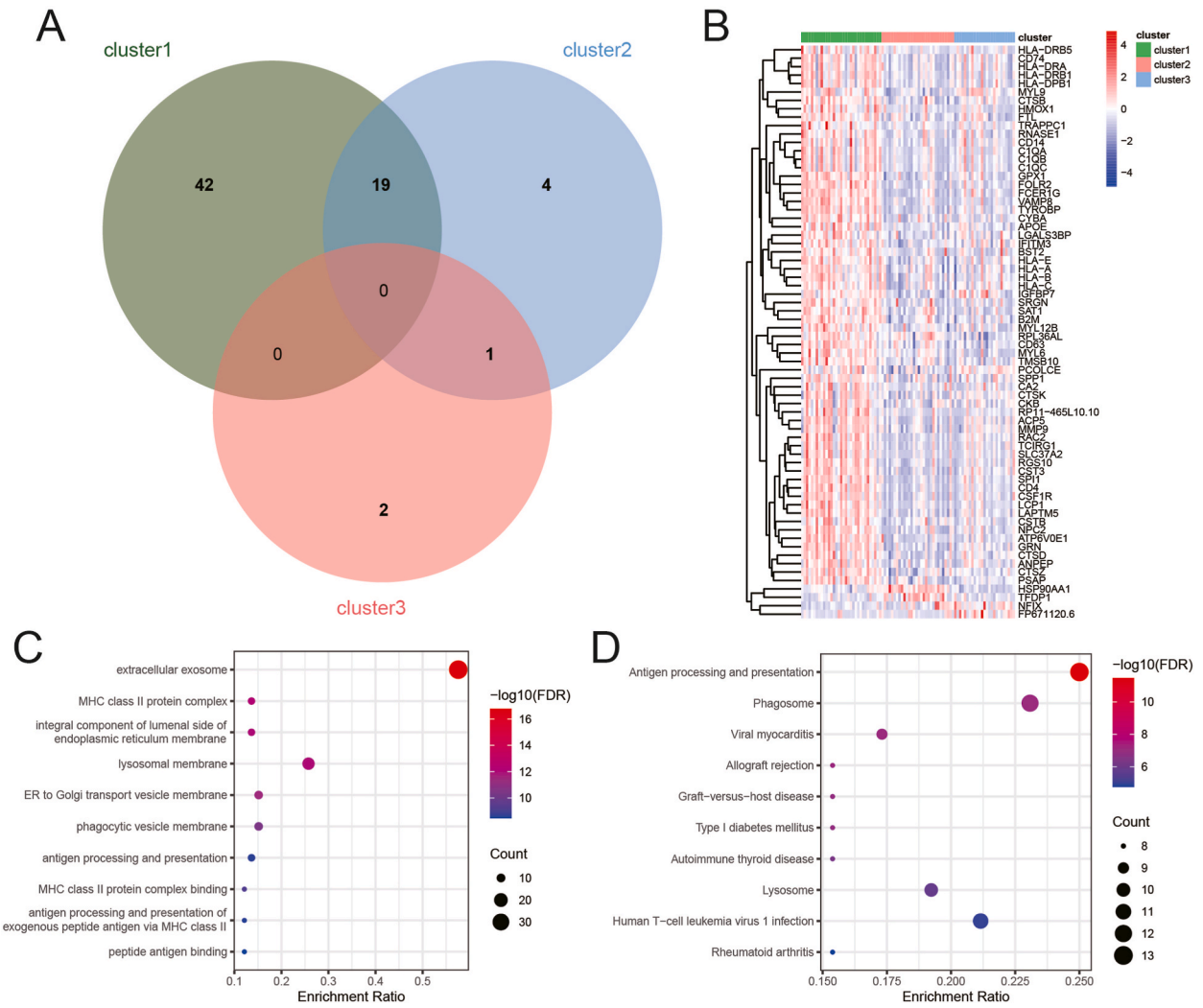

Fig. 4. Differential expression analysis among three clusters in TARGET dataset. (A) Venn plot of DEGs among three clusters. (B) A heatmap showing the expression of 68 DEGs. (C–D) The top 10 enriched GO terms and KEGG pathways of DEGs.

3.4. Establishing an ICD risk signature

Subsequently, a prognostic model using ICD-related genes was created. Univariate Cox regression analysis determined 5 prognostic genes from the 34 ICD-correlated genes. TLR4, LY96, IFNGR1, CD4, and CASP1 expression levels were negatively correlated with the overall survival (HR < 1, Fig. 5A), indicating that they could serve as protective factors of osteosarcoma. To establish the risk signature, we performed LASSO to obtain the coefficients of each prognostic gene (Fig. 5B and C). Each sample was calculated with a risk score according to the ICD risk signature. According to the median cut-off value of −1.378, two risk groups (low and high) of osteosarcoma samples were categorized. High-risk group had obviously more dead samples and lower expression of the five prognostic genes than low-risk group (Fig. 5D). In TARGET and GSE21257 datasets, two risk groups all showed different overall survival with P = 0.0031 and P = 0.045 respectively (Fig. 5E and F).

3.5. Validation of ICD risk signature predicting the progress of osteosarcoma

To validate the reliability of ICD risk signature in predicting the prognosis of osteosarcoma and to unearth key ICD-related genes significantly associated with the malignant phenotype of osteosarcoma, we used PCR to detect the expression of TLR4, LY96, IFNGR1, CD4, and CASP1 in normal osteoblasts hFOB1.19 as well as in MG-63 and Saos-2 cell lines. The results showed that compared to normal osteoblast hFOB1.19, five genes (TLR4, LY96, IFNGR1, CD4, and CASP1) were all decreased in expression in MG-63 and Saos-2 cell lines (Fig. 6A-E). Next, we selected the molecule LY96 for subsequent experiments. After overexpression of LY96 in the two cell lines, the migratory and invasive abilities of the two cell lines were significantly reduced (Fig. 6F and G). The results of CCK8 also showed a

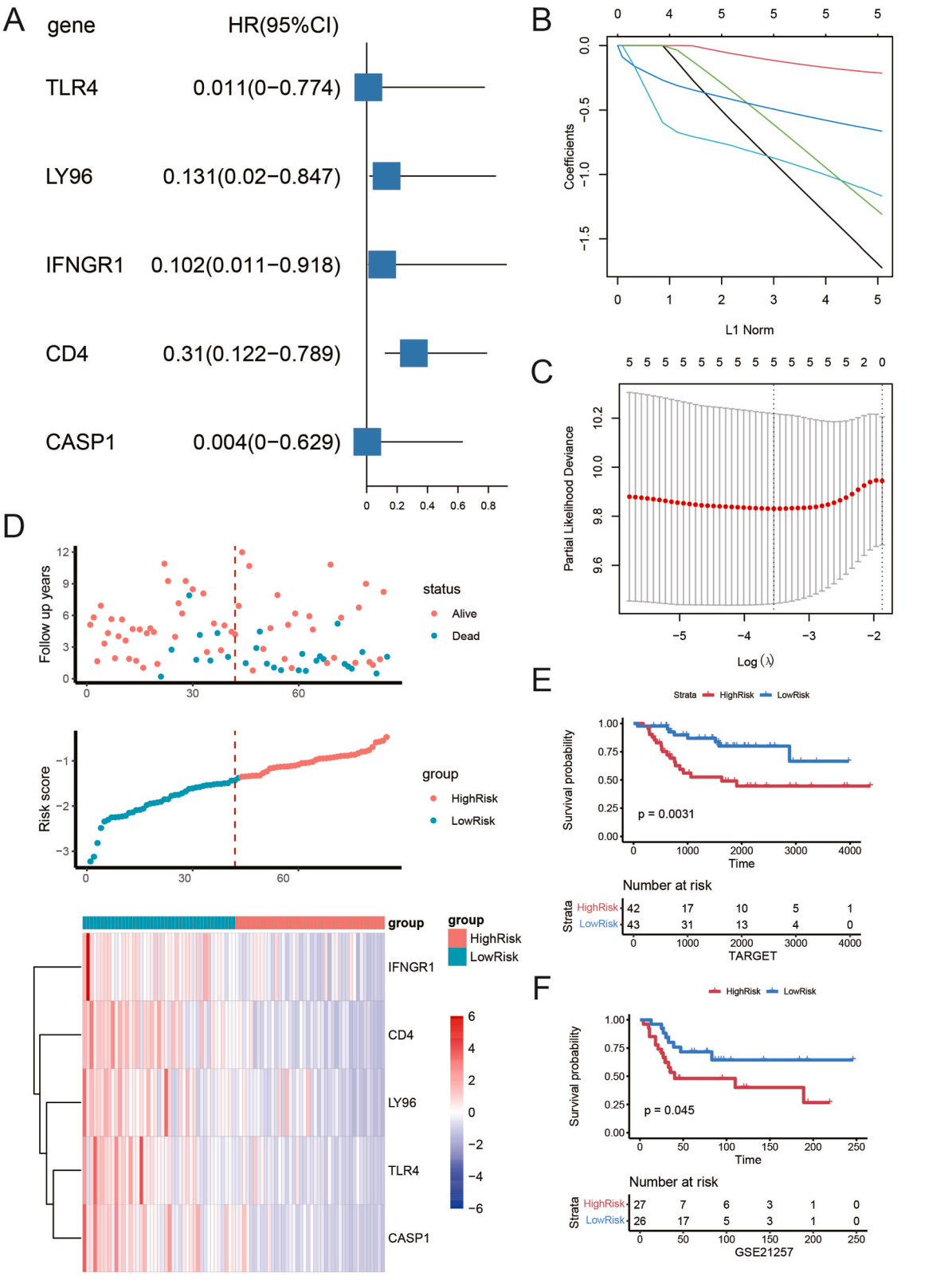

(caption on next page)

Fig. 5. Establishment and validation of the ICD-related risk signature. (A) Univariate Cox regression analysis of 34 ICD-related genes in TARGET dataset. The result of five prognostic genes was shown. The horizontal axis indicates the hazard ratio (HR). (B–C) LASSO Cox regression analysis of five prognostic genes in TARGET dataset. (D) The distribution of samples ranked by the risk score, and the expression of five prognostic genes in TARGET dataset. (E–F) KM survival curves of high-risk and low-risk groups in TARGET and GSE21257 datasets. Log-rank test was conducted.

decrease in cell viability in the two cell lines after overexpression of LY96 in the two cell lines (Fig. 7A and B). The cell cycle results showed an increase in the ratio of S Phase and a prolongation of S Phase in the two cell lines after overexpression of LY96 (Fig. 7C and D).

3.6. The potential of the ICD risk signature for guiding immunotherapy

The ICD risk score and immune cell infiltration was examined to evaluate the clinical value of ICD risk signature in immunotherapy. The risk score was negatively correlated with CD8 T cells (R = −0.23), neutrophils (R = −0.28), M1 macrophages (R = −0.24), and M2 macrophages (R = −0.39), and was positively correlated with naïve CD4 T cells (R = 0.30) and M0 macrophages (R = 0.42), as revealed by Pearson correlation analysis (P < 0.05, Fig. 8A–F). Then we used to TIDE in response prediction of immune checkpoint

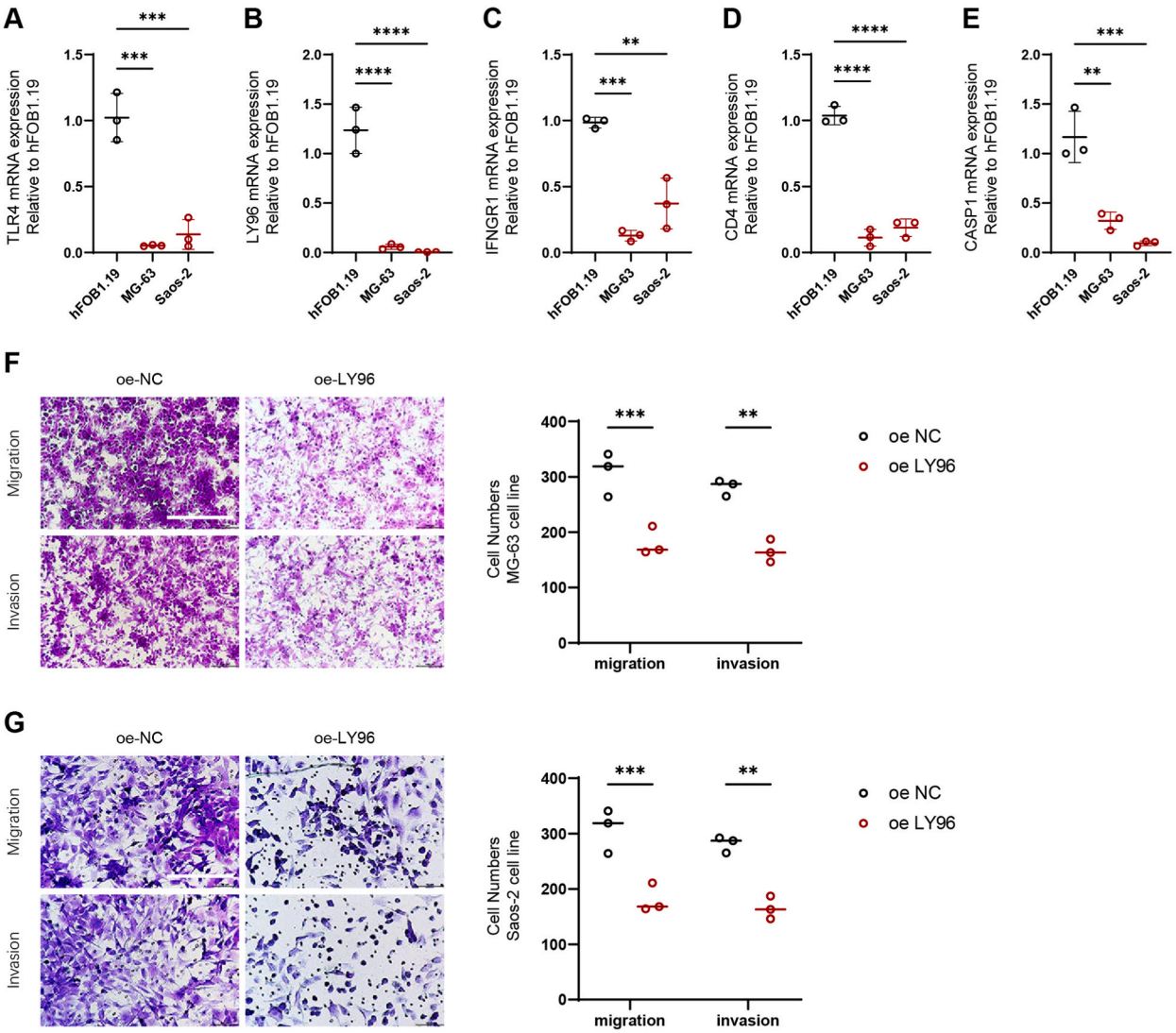

Fig. 6. Validation of bioinformatics results. (A–E) PCR was performed to detect the expression of TLR4, LY96, IFNGR1, CD4, and CASP1 in MG-63, Saos-2 and hFOB1.19 cell lines, and relative quantification was performed. (n = 3). (F–G) Alterations in cell migration and invasive capacity following overexpression of LY96 expression in MG-63 and Saos-2 cell lines and quantification of cell numbers. (n = 3). *≤0.05, **≤0.01 , ***≤0.001 , ****≤0.0001. N = 3, The results are presented as mean ± SD.

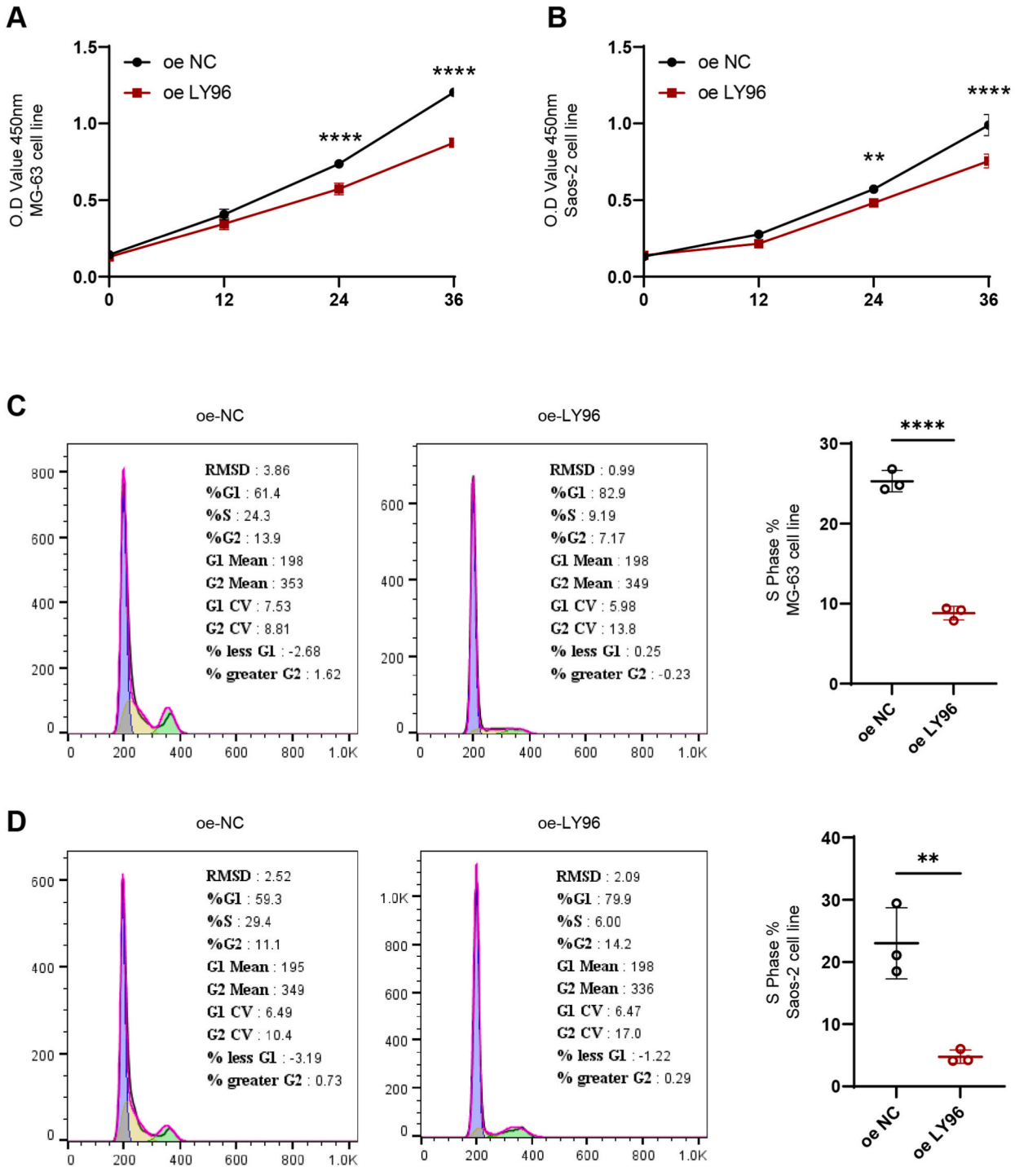

Fig. 7. LY96 inhibits the development of osteosarcoma. (A–B) Changes in cell viability from 0 to 36h after overexpression of LY96 expression in MG-63 and Saos-2 cell lines and quantification of O.D Value. (n = 3). (C–D) Changes in cell cycle after overexpression of LY96 expression in MG-63 and Saos-2 cell lines and quantification of O.D Value. (n = 3). *≤0.05, **≤0.01 , ***≤0.001 , ****≤0.0001. N = 3, The results are presented as mean ± SD.

blockade. The result showed a significantly higher TIDE score of low-risk group, implying a high possibility of immune escape (Fig. 8G). Furthermore, the risk score showed an obviously higher HR than other clinical features (compared with gender, age, race) (HR = 3.811, 95%CI = 1.633–8.895). The above results showed that the ICD risk signature was reliable to be a prognostic indicator for osteosarcoma and may also serve as an indicator for evaluating patients' immunotherapy response.

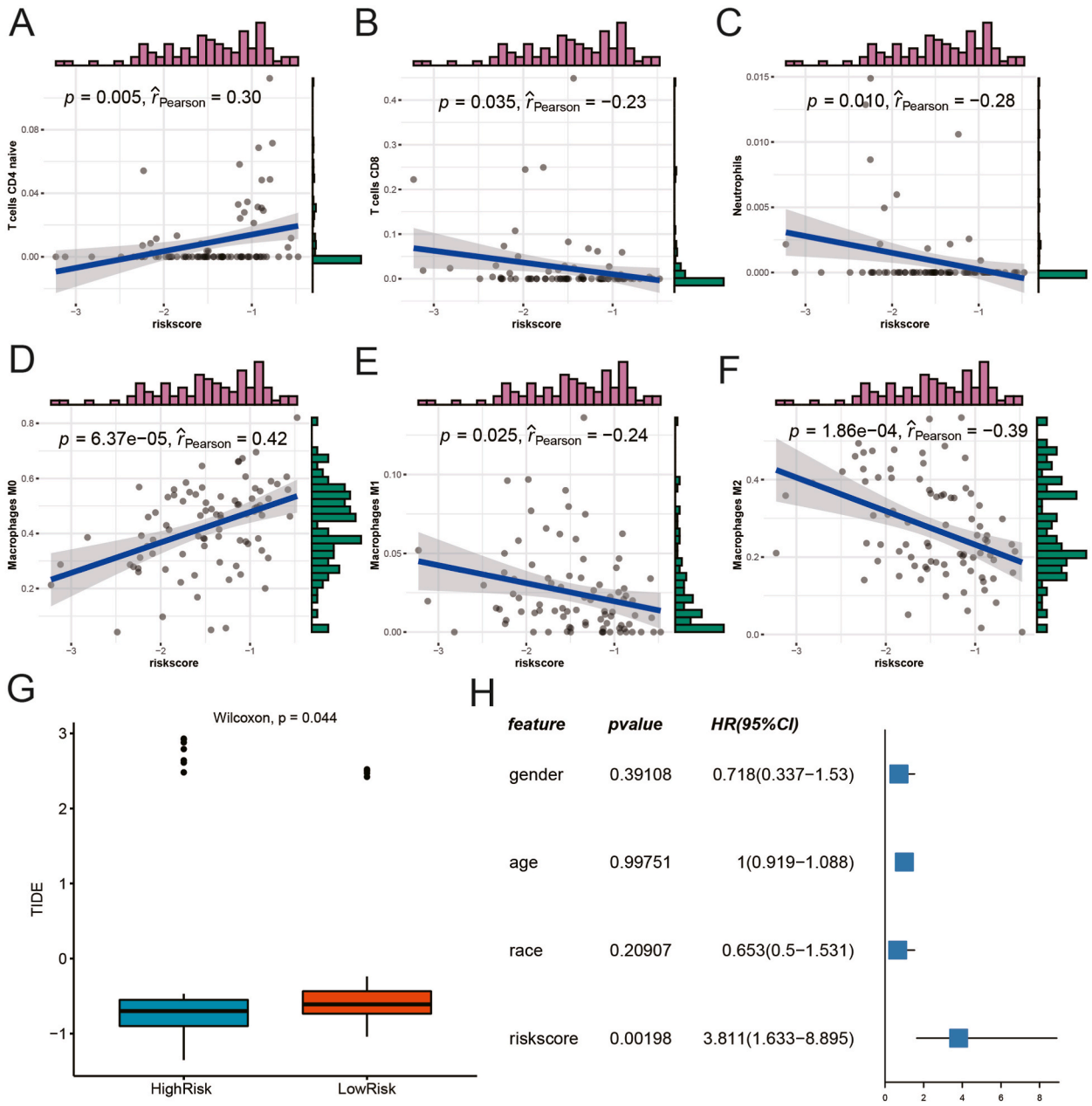

Fig. 8. The relation between the risk score and immune microenvironment. (A–F) Pearson correlation analysis between the risk score and the enrichment of immune cells. (G) TIDE analysis of two risk groups. Wilcoxon test was conducted. (H) The risk score and clinical features analyzed by Univariate Cox regression analysis. Log-rank test was conducted.

4. Discussion

Lines of evidences have corroborated that ICD can elicit anti-cancer activity in combination with chemotherapeutic drugs and immune checkpoint inhibitors [42,43]. For example, in a combined therapy of dendritic cells and doxorubicin, enhanced anti-cancer effects induced by ICD was shown in osteosarcoma [44]. DAMPs releasing from dying cancer cells can be recognized by Toll-like receptors and NOD-like receptors (NLRs) that stimulate the innate and adaptive immune response and ultimately initiate tumor-specific $CD8^+$ T cells to kill cancer cells [42,45,46]. There are also preclinical and clinical evidence suggest that DAMPs and DAMP-associated process including CALR and HSP signaling have a potential to serve as prognostic indicators for cancer patients [47–50]. Enlightened by the previous research, we believe that there is a potential value of ICD-correlated genes in cancer prognosis prediction. However, the association between these genes and osteosarcoma prognosis has not been comprehensively studied.

The present work evaluated the expression profiles of 34 ICD-correlated genes in osteosarcoma samples and discovered that nine

DEGs between normal and tumor samples. The differential genes are *IL1B*, *NLRP3*, *EIF2AK3*, *CASP8*, *NT5E*, *MYD88*, *CALR*, *CD4* and *IL1R*. We identified three clusters (or molecular subtypes) based on the expression of 34 ICD-correlated genes. Notably, cluster1 had the longest overall survival and obviously high expression of ICD-related genes, compared with other two clusters. The ICD activation process induces a strong immune response against tumor cells by promoting antigen presentation and enhancing T cell activation. This immune response induced by ICD is often associated with a better cancer prognosis, as it helps to clear tumor cells and reduces the likelihood of recurrence [51]. ICD induces the recruitment and activation of antigen-presenting cells, and thus activates the anti-cancer response [52]. The above results clarified the association between ICD and osteosarcoma, and supported the reliability of molecular subtyping based on ICD-related genes. The above observation suggested that the active ICD process was associated with favorable prognosis.

Furthermore, we established an ICD-related risk signature using ICD-correlated genes, and *TLR4*, *LY96*, *IFNGR1*, *CD4*, and *CASP1* were identified as prognostic genes. According to accumulated evidence, *TLR4, IFNGR1*, *CD4*, and *CASP1* were related to the progression of Osteosarcoma. *TLR4* was identified as a regulatory factor in the invasion and migration processes of osteosarcoma. Studies had found that *LPS* could activate the expression of *TLR4*, which then acted on HOTAIR to promote the invasion and migration of osteosarcoma [53]. The upregulation of *IFNGR* expression was able to synergistically enhance the chemokine response to exogenous *IFN*, triggering the activity of NK cells in pediatric bone cancer [54]. *CD4* was identified as a key target in osteosarcoma research, with its expression in osteosarcoma cells being lower compared to osteoblasts, indicating its potential role in the immune regulation of osteosarcoma development. Additionally, the binding potential of *CD4* with specific drugs suggested that it could serve as a potential target for osteosarcoma treatment [55]. *CASP1* was identified as an osteosarcoma-specific interaction pair, and as a significant factor in the development of osteosarcoma, it could influence the pathological process of osteosarcoma through its specific interactions and involvement in regulating the FGFR, MAPK, and Notch signaling pathways [56]. Although there were no reports of I*FNGR1* in osteosarcoma, IFNGR1 was a poor prognostic marker for the metastasis of prostate cancer [57]. From these studies, it was evident that the prognostic genes with ICD characteristics in osteosarcoma were closely related to its development, and using these genes as prognostic features was justified. Secondly, these genes are associated with osteosarcoma metastasis and invasion, and they may be potential novel targets. Focusing on these prognostic genes in the future is expected to provide new insights into the development of new targeted treatment technologies for osteosarcoma.

In addition, according to our results, ICD risk profile showed a significant positive trend with CD8 T cells. High-risk group is more sensitive to immunotherapy.CD8+ T cells play a central role in cancer immunotherapy. They are the most powerful effectors of the adaptive immune system in the immune response against cancer and form the basis of current successful cancer immunotherapies. CD8+ T cells, which exert their effects by recognizing and killing cancer cells presenting specific antigens, are the immune cells of choice against cancer. However, during cancer progression, $CD8^+$ T cells experience dysfunction and depletion due to immune-associated tolerance and immunosuppression within the tumor microenvironment, thus compromising their ability to clear tumors. Immune checkpoint inhibitors are designed to target immunosuppressive receptors that modulate immune responses, whereas adoptive cell transfer therapies use $CD8^+$ T cells with genetically modified receptors, such as chimeric antigen receptors, to specify and enhance $CD8^+$ T cell function. By activating $CD8^+$ T cells, the immune checkpoint blockade (ICB) strategy improves the ratio of co-stimulatory to co-inhibitory mediators, PD-1/PD-L1 and CTLA-4 being the checkpoint receptors that can be targeted to alleviate the depletion of $CD8^+$ T cells and renew their activation, thereby eliminating the antigen-expressing cancer cells [58,59]. This is consistent with our trend that $CD8^+$ T cells are more abundant in High-risk group. Moreover, in our study, the TIDE score was lower in the High-risk group, suggesting that immune escape was less pronounced.

Osteosarcoma samples were classified into two risk groups, and low-risk group exhibited significantly higher levels of expression of these genes, which was consistent with the previous observation in cluster1. We validated the risk signature in two dependent datasets and the consistent results were shown, suggesting that the five-gene signature was robust and effective in predicting the prognosis for osteosarcoma patients. Notably, in the response to immune checkpoint inhibitors, low-risk group may benefit much from the immunotherapy. Besides the prognosis prediction, the risk signature also had a potential to indicate the anti-cancer response to immune checkpoint inhibitors.

However, this study only used the pure bioinformatics analysis coupled with a series of basic cell experiments and the results need further verifications in the in-depth experiments. Besides, due to the relatively low incidence of osteosarcoma, the samples were not abundant and this may affect the accuracy of the results. Furthermore, we did not consider the age or other factors that may have an effect on the osteosarcoma development and ICD process.

5. Conclusions

In conclusion, this study found an association between ICD and osteosarcoma prognosis. High activity of ICD was shown in osteosarcoma patients with good prognosis. ICD-related characteristic genes are led to malignant phenotypes of osteosarcoma cell lines including migration, invasion, viability and cell cycle. Cluster1 had higher immune infiltration and higher expression of HLA-correlated genes. Moreover, we constructed an ICD-correlated risk signature that was effective to evaluate the prognosis of osteosarcoma patients and the risk signature was potential to guide personalized immunotherapy or ICD-related therapy.

Funding

The present study was supported by the National Natural Science Youth Fund (82,003,132), Excellent young medical talents training program in Pudong New Area health system (PWRq2021–33), long voyage plan of Shanghai Pudong New Area People's

Hospital (PRYYH202301), Key Specialty of Pudong New Area Health Commission (PWZxk2022-16) and Project of Clinical Outstanding Clinical Discipline Construction in Shanghai Pudong New Area (PWYgy2021-08).

Ethics statement

N/A.

Data Availability Statement

The data that support the findings of this study are openly available in [GSE126209] at [https://www.ncbi.nlm.nih.gov/geo/query/acc.cgi?acc=GSE126209], in [GSE21257] at [https://www.ncbi.nlm.nih.gov/geo/query/acc.cgi?acc=GSE21257].

Consent for publication

All authors have read and agreed to publish the article.

CRediT authorship contribution statement

Shuai Han: Writing – review & editing, Writing – original draft, Visualization, Methodology, Funding acquisition. **Qinghe Wang:** Writing – review & editing, Writing – original draft, Visualization, Project administration, Investigation. **Mingquan Shen:** Writing – review & editing, Writing – original draft, Supervision, Software, Investigation, Data curation. **Xingpeng Zhang:** Validation, Software, Project administration, Formal analysis. **Jian Wang:** Writing – review & editing, Validation, Resources, Project administration, Funding acquisition, Conceptualization.

Declaration of competing interest

The authors declare that they have no known competing financial interests or personal relationships that could have appeared to influence the work reported in this paper.

Acknowledgement

None.

Abbreviations

CDF	Cumulative distribution function
DAMPs	Damage-associated molecular patterns
DEGs	Differentially expressed genes
FDR	False discovery rate
GEO	Gene Expression Omnibus
GO	Gene Ontology
HR	Hazard ratio
HLA	Human leukocyte antigen
ICD	Immunogenic cell death
KEGG	Kyoto Encyclopedia of Genes and Genomes
LASSO	Least absolute shrinkage and selection operator
PPI	Protein-protein interaction
TIDE	Tumor Immune Dysfunction and Exclusion
TME	Tumor microenvironment

References

[1] Y. Zhang, et al., Progress in the chemotherapeutic treatment of osteosarcoma, Oncol. Lett. 16 (5) (2018) 6228–6237.
[2] S. Li, et al., Targeted therapy for osteosarcoma: a review, J. Cancer Res. Clin. Oncol. 149 (9) (2023) 6785–6797.
[3] L. Mirabello, R.J. Troisi, S.A. Savage, Osteosarcoma incidence and survival rates from 1973 to 2004: data from the surveillance, epidemiology, and end results program, Cancer 115 (7) (2009) 1531–1543.
[4] Z. Shoaib, T.M. Fan, J.M.K. Irudayaraj, Osteosarcoma mechanobiology and therapeutic targets, Br. J. Pharmacol. 179 (2) (2022) 201–217.
[5] L. Tang, et al., Expression and clinical significance of ACTA2 in osteosarcoma tissue, Oncologie 24 (4) (2022).
[6] B.A. Lindsey, J.E. Markel, E.S. Kleinerman, Osteosarcoma overview, Rheumatol Ther 4 (1) (2017) 25–43.

[7] J Zou, L Chen, H Xu, Unveiling and validation of a disulfidptosis determined prognostic model for osteosarcoma: new insights from prognosis to immunotherapy and chemotherapy, Oncologie 25 (4) (2023) 417–433. https://doi.org/10.1515/oncologie-2023-0129.
[8] J. Tan, et al., Circular RNA circEMB promotes osteosarcoma progression and metastasis by sponging miR-3184-5p and regulating EGFR expression, Biomark. Res. 11 (1) (2023) 3.
[9] A. Misaghi, et al., Osteosarcoma: a comprehensive review, Sicot j 4 (2018) 12.
[10] F. Eilber, et al., Adjuvant chemotherapy for osteosarcoma: a randomized prospective trial, J. Clin. Oncol. 5 (1) (1987) 21–26.
[11] H. Zhang, et al., Expression Changes, prognostic analysis and risk factors of miR-625-3p and miR-449a in osteosarcoma patients after surgery, Oncologie 22 (1) (2020) 23–33.
[12] F. Jafari, et al., Osteosarcoma: a comprehensive review of management and treatment strategies, Ann. Diagn. Pathol. 49 (2020) 151654.
[13] L. Kager, et al., Primary metastatic osteosarcoma: presentation and outcome of patients treated on neoadjuvant Cooperative Osteosarcoma Study Group protocols, J. Clin. Oncol. 21 (10) (2003) 2011–2018.
[14] Y. Yuan, et al., Peptide-based semiconducting polymer nanoparticles for osteosarcoma-targeted NIR-II fluorescence/NIR-I photoacoustic dual-model imaging and photothermal/photodynamic therapies, J Nanobiotechnology 20 (1) (2022) 44.
[15] S. Miwa, et al., Current and emerging targets in immunotherapy for osteosarcoma, J Oncol 2019 (2019) 7035045.
[16] Z. Zhang, et al., Characterization of the tumour microenvironment phenotypes in malignant tissues and pleural effusion from advanced osteoblastic osteosarcoma patients, Clin. Transl. Med. 12 (11) (2022) e1072.
[17] S. Wang, et al., Myeloid-derived suppressor cells: key immunosuppressive regulators and therapeutic targets in hematological malignancies, Biomark. Res. 11 (1) (2023) 34.
[18] Z. Chen, et al., Nanomaterials: small particles show huge possibilities for cancer immunotherapy, J Nanobiotechnology 20 (1) (2022) 484.
[19] R. Huang, et al., Adoptive neoantigen-reactive T cell therapy: improvement strategies and current clinical researches, Biomark. Res. 11 (1) (2023) 41.
[20] S. Miwa, et al., Phase 1/2 study of immunotherapy with dendritic cells pulsed with autologous tumor lysate in patients with refractory bone and soft tissue sarcoma, Cancer 123 (9) (2017) 1576–1584.
[21] N. Ahmed, et al., Human epidermal growth factor receptor 2 (HER2) -specific chimeric antigen receptor-modified T cells for the immunotherapy of HER2-positive sarcoma, J. Clin. Oncol. 33 (15) (2015) 1688–1696.
[22] H.A. Tawbi, et al., Pembrolizumab in advanced soft-tissue sarcoma and bone sarcoma (SARC028): a multicentre, two-cohort, single-arm, open-label, phase 2 trial, Lancet Oncol. 18 (11) (2017) 1493–1501.
[23] K. Yoshida, et al., Clinical outcome of osteosarcoma and its correlation with programmed death-ligand 1 and T cell activation markers, OncoTargets Ther. 12 (2019) 2513–2518.
[24] K. Yoshida, et al., A review of T-cell related therapy for osteosarcoma, Int. J. Mol. Sci. 21 (14) (2020).
[25] L. Galluzzi, et al., Immunogenic cell death in cancer: concept and therapeutic implications, J. Transl. Med. 21 (1) (2023) 162.
[26] A. Ahmed, S.W.G. Tait, Targeting immunogenic cell death in cancer, Mol. Oncol. 14 (12) (2020) 2994–3006.
[27] H. Ruan, et al., Immunogenic cell death in colon cancer prevention and therapy, Mol. Carcinog. 59 (7) (2020) 783–793.
[28] X. Xu, et al., Fabrication of methylene blue-loaded ovalbumin/polypyrrole nanoparticles for enhanced phototherapy-triggered antitumour immune activation, J Nanobiotechnology 20 (1) (2022) 297.
[29] L. Galluzzi, et al., Immunostimulation with chemotherapy in the era of immune checkpoint inhibitors, Nat. Rev. Clin. Oncol. 17 (12) (2020) 725–741.
[30] J. Pol, et al., Trial Watch: immunogenic cell death inducers for anticancer chemotherapy, OncoImmunology 4 (4) (2015) e1008866.
[31] Z. Asadzadeh, et al., Current approaches for combination therapy of cancer: the role of immunogenic cell death, Cancers 12 (4) (2020).
[32] A.D. Garg, D. De Ruysscher, P. Agostinis, Immunological metagene signatures derived from immunogenic cancer cell death associate with improved survival of patients with lung, breast or ovarian malignancies: a large-scale meta-analysis, OncoImmunology 5 (2) (2016) e1069938.
[33] M.D. Wilkerson, D.N. Hayes, ConsensusClusterPlus: a class discovery tool with confidence assessments and item tracking, Bioinformatics 26 (12) (2010) 1572–1573.
[34] K. Yoshihara, et al., Inferring tumour purity and stromal and immune cell admixture from expression data, Nat. Commun. 4 (2013) 2612.
[35] B. Chen, et al., Profiling tumor infiltrating immune cells with CIBERSORT, Methods Mol. Biol. 1711 (2018) 243–259.
[36] P. Jiang, et al., Signatures of T cell dysfunction and exclusion predict cancer immunotherapy response, Nat. Med. 24 (10) (2018) 1550–1558.
[37] M.E. Ritchie, et al., Limma powers differential expression analyses for RNA-sequencing and microarray studies, Nucleic Acids Res. 43 (7) (2015) e47.
[38] G. Yu, et al., clusterProfiler: an R package for comparing biological themes among gene clusters, OMICS 16 (5) (2012) 284–287.
[39] J. Friedman, T. Hastie, R. Tibshirani, Regularization paths for generalized linear models via coordinate descent, J Stat Softw 33 (1) (2010) 1–22.
[40] W. Shen, et al., Sangerbox: a comprehensive, interaction-friendly clinical bioinformatics analysis platform, iMeta (2022), https://doi.org/10.1002/imt2.36.
[41] P. Hernández A, et al., Restoring the immunity in the tumor microenvironment: insights into immunogenic cell death in onco-therapies, Cancers 13 (11) (2021).
[42] J. Fucikova, et al., Detection of immunogenic cell death and its relevance for cancer therapy, Cell Death Dis. 11 (11) (2020) 1013.
[43] J. Zhou, et al., Immunogenic cell death in cancer therapy: present and emerging inducers, J. Cell Mol. Med. 23 (8) (2019) 4854–4865.
[44] M. Kawano, et al., Dendritic cells combined with doxorubicin induces immunogenic cell death and exhibits antitumor effects for osteosarcoma, Oncol. Lett. 11 (3) (2016) 2169–2175.
[45] N. Yatim, S. Cullen, M.L. Albert, Dying cells actively regulate adaptive immune responses, Nat. Rev. Immunol. 17 (4) (2017) 262–275.
[46] T. Gong, et al., DAMP-sensing receptors in sterile inflammation and inflammatory diseases, Nat. Rev. Immunol. 20 (2) (2020) 95–112.
[47] J. Fucikova, et al., Prognostic and predictive value of DAMPs and DAMP-associated processes in cancer, Front. Immunol. 6 (2015) 402.
[48] M.P. Chao, et al., Calreticulin is the dominant pro-phagocytic signal on multiple human cancers and is counterbalanced by CD47, Sci. Transl. Med. 2 (63) (2010) 63ra94.
[49] J.S. Chen, et al., Secreted heat shock protein 90alpha induces colorectal cancer cell invasion through CD91/LRP-1 and NF-kappaB-mediated integrin alphaV expression, J. Biol. Chem. 285 (33) (2010) 25458–25466.
[50] R.Q. Peng, et al., Expression of calreticulin is associated with infiltration of T-cells in stage IIIB colon cancer, World J. Gastroenterol. 16 (19) (2010) 2428–2434.
[51] X. Niu, et al., Ferroptosis, necroptosis, and pyroptosis in the tumor microenvironment: perspectives for immunotherapy of SCLC, Semin. Cancer Biol. 86 (Pt 3) (2022) 273–285.
[52] G. Kroemer, et al., Immunogenic cell stress and death, Nat. Immunol. 23 (4) (2022) 487–500.
[53] N. Wang, et al., LPS promote Osteosarcoma invasion and migration through TLR4/HOTAIR, Gene 680 (2019) 1–8.
[54] I.C. Henrich, et al., Ubiquitin-specific protease 6 functions as a tumor suppressor in ewing sarcoma through immune activation, Cancer Res. 81 (8) (2021) 2171–2183.
[55] Y. Wang, et al., Identification of therapeutic targets for osteosarcoma by integrating single-cell RNA sequencing and network pharmacology, Front. Pharmacol. 13 (2022) 1098800.
[56] H. Li, et al., Identification of characteristic gene modules of osteosarcoma using bioinformatics analysis indicates the possible molecular pathogenesis, Mol. Med. Rep. 15 (4) (2017) 2113–2119.
[57] M.G. Ferrari, A.P. Jimenez-Uribe, L. Wang, L.H. Hoeppner, P. Murugan, E. Hahm, J. Yu, T.M. Kuzel, S.A. Gradilone, A.P. Mansini, Myeloid differentiation factor-2/LY96, a potential predictive biomarker of metastasis and poor outcomes in prostate cancer: clinical implications as a potential therapeutic target, Oncogene 43 (7) (2024 Feb) 484–494, https://doi.org/10.1038/s41388-023-02925-x. Epub 2023 Dec 23. PMID: 38135694; PMCID: PMC10857939.
[58] B. Farhood, M. Najafi, K. Mortezaee, CD8(+) cytotoxic T lymphocytes in cancer immunotherapy: a review, J. Cell. Physiol. 234 (6) (2019) 8509–8521.
[59] H. Kogo, et al., Suppression of murine tumour growth through CD8(+) cytotoxic T lymphocytes via activated DEC-205(+) dendritic cells by sequential administration of alpha-galactosylceramide in vivo, Immunology 151 (3) (2017) 324–339.